Three-dimensional printed thermoplastic polyurethane on fabric as wearable smart sensors

Abstract: The microstrip patch antenna (MPA) with a thermoplastic substrate has been widely used in wearable sensors primarily due to its lightweight, flexibility, strength, and compactness. But up till now, little has been conveyed on the use of three-dimensional (3D) printed thermoplastic polyurethane (TPU) on cotton-lycra woven (CLW) fabric-based substrate as a wearable sensor. This study presents a novel and scalable approach for characterizing, simulating, and fabricating the substrate for wearable sensor applications. In this study 3D printing of TPU on CLW fabric (70% cotton (on the warp side)-30% lycra (on the weft side) using fused filament fabrication (FFF) process) has been reported with a tradeoff between flexibility and strength (of a substrate for wearable sensor applications). The rheological, mechanical, morphological, four-dimensional (4D), and resonance frequency (RF) characterization of the substrate has been established. As regards rheological properties, the melt flow index (MFI) of primary (1°) recycled TPU was observed as 29.758 g/(10min). Further, the optimized 3D printing settings of TPU were obtained based on the mechanical testing (minimum stiffness, maximum peak strength (PS), maximum Young's modulus (E), and maximum strain energy (SE)) which comes out to be 225°C nozzle temperature, 18 mm/s printing speed and 60% infill density with a stiffness of 3.311 N/mm and PS of 9.628 MPa. The mechanical properties of TPU printed on stretched and unstretched CLW fabric were tested for lower stiffness (more flexibility). To ascertain the mechanical properties, porosity analyses of samples printed on CLW fabric have been performed based on scanning electron microscopy (SEM). For dielectric properties, and RF characterization, the ring resonator (RR) test was performed based on a Vector network analyzer (VNA). Finally, 4D characterization of the substrate was performed by applying a load from 0-25 N, resulting in programable RF output (in the industry scientific and medicine (ISM) band).

Keywords: Thermoplastic polyurethane; cotton-lycra woven fabric; 3D printing; wearable; smart sensor; VNA; mechanical properties

Introduction: In recent years, the miniaturization of electronics has fueled wearable technology leading to the great interest of researchers in wearable devices [1]. Wearable sensors have an important role in the advancement, adaptability, and capabilities of the internet of things (IoT) based solutions [2, 3]. Commercially, the use of wearable sensors in smart glasses and smartwatches has gained popularity because of their attractive design and practical user interface [3]. The important consideration of wearable antennas or wearable sensors is being inconspicuous arising the need to be integrated within the clothing causing minimal interference with the usual routine of the user and negating the inconvenience in daily activities [4]. Integrating the sensors with fabrics (clothes) impacts modern-day life providing different military and medical applications including heart or brain disorder analyses etc. [5]. Researchers have shown great interest in the field of wearable sensors (sensors integrated into clothes) such as armbands [6], caps and clothes, etc. [7]. Wearable antennas have applications in the body area network (BAN) for reliable and robust connectivity between bodies providing massive IoT to monitor the health parameters such as pulse rate, body temperature, location of a user, etc. [8]. The wearable sensors should be flexible providing conformability, easy bending, wrinkling, etc. to provide easy application on fabrics [9].

The antenna, a vital component of wearable devices, integrated with the clothes must be light in weight, conformal, and should be able to withstand mechanical stress. MPA is one of the best choices to fulfill these preferred options for wearable applications due to its simple construction, low cost, and lightweight. An MPA consists of three parts namely: (i) patch or radiating part, (ii) ground, and (iii) substrate. The metallic ground shows an advantage in wearable applications by significantly reducing the energy absorbed by the user's body by deflecting the radiations coming from radiating patches [10]. The substrates of the MPA need to be flexible to provide mobility in wearable sensors. The researchers have

experimented with different materials including textiles, plastic, polymers, paper, and fabrics to increase the flexibility of electronic systems. The used materials have their unique properties in terms of how they can be bent or twisted [11]. A considerable amount of work has been reported on designing flexible wearable antennas using textiles [12], paper [13], and synthesized substrates [14] but the thickness of textile and paper substrates is limited and has high fluid absorption. The textiles have low relative permittivity which can be improved by printing a flexible polymer on the textile using FFF with a little compromise in flexibility. It was also studied that the relative permittivity of the human body and its lossy material can affect the antenna performance and efficiency. To reduce the effects of radiation on the human body and the effect of the human body on antenna performance multilayer structures have been explored in previous studies [15].

Several additive manufacturing (AM) technologies have been developed in the recent past, but one of the most cost-effective and most-used techniques is FFF [16, 17]. FFF prints the parts layer-by-layer deposition of fused material [18]. Numerous publications have classified the FFF as one of the best technologies for sensor fabrication [19]. This process allows variation in the internal structure, to alter the dielectric properties of the substrate (while fabricating the complex shapes). FFF has been widely used for printing substrates for the MPA with customized structures [20]. It was studied that the addition of air inclusions inside the material decreases its relative permittivity whereas metallic or high permittivity inclusions increase the relative permittivity of the material [21]. Applications of AM in the field of antennas have opened an interdisciplinary field for material science and electronics [22]. The FFF has been used for substrate printing for the MPA using polylactic acid (PLA), acrylonitrile butadiene styrene (ABS) and Ninja flex, etc. [23]. Studies have also shown that all parts of MPA (patch, substrate, and ground) have also been printed using AM techniques [24]. Different AM techniques such as inkjet 3D printing have shown their application in the field of textile wearable sensors [25] such as printing antennas on leather bags [26], watches and armbands, etc. Numerous studies have used 3D-printed ABS and PLA as a substrate for MPA but their non-stretchability and non-flexibility have obliterated them in wearable applications [27]. Ninja flex has been printed directly on fabrics using FFF for wearable sensors due to its flexibility [28]. TPU has properties such as good flexibility, recyclability stretchability, and good mechanical properties which makes TPU one of the perfect polymers to be printed on textiles for wearable sensor applications [29]. TPU already has been widely used in footwear, automotive, sports goods, hose, pipe, and cable industries [30]. The shape recoverability of TPU opens its application in the field of 4D printing [31]. A wearable MPA by printing TPU on FFF has been developed by researchers for breast hyperthermia [32]. A co-planar waveguide antenna has been fabricated on a cotton layer for wearable applications [33]. Researchers also have developed a washable wearable antenna with a covering of TPU using an inkjet printer [7]. A wearable antenna has been simulated and designed for a resonating frequency of 2.45GHz using jeans as a substrate and copper tape as a conductive part [10]. The 4D printed sensor has been fabricated from a thermo-deformable bow-tie antenna for special applications in changing antenna properties [34]. Jeans substrate with a dielectric constant (ε_r) of 1.78 has been used as a substrate for wearable MPA operating at a RF of 5.8GHz and electro textile has been used as conductive material [35]. A study for direct printing of PLA on the cotton fabric has been performed by using FFF (by varying the nozzle diameter, nozzle temperature, and distance between the nozzle and bed) [36]. It was also found that woven fabric has shown better adhesion as compared to the knitted fabric when PLA was directly printed [37]. In most of the reported studies, only textile-based substrates have been used for wearable sensors [38] but they have low relative permittivity and low robustness. In one of the recent studies, TPU was 3D printed on three textile materials, a knitted fabric from 100 % polyester (PES) (thickness d = 0.79 mm), a woven fabric from 100 % PES (d = 0.27 mm), and a woven fabric from 100 % cotton (d = 0.19 mm) and the adhesion of 3D printed substrate was examined after the different number of cycles [39]. In a similar study, PLA and TPU were printed on woven lycra net with FFF for wearable sensor applications. Further, the adhesiveness between the fabric and polymer was tested by tensile test and warping. The results have shown the better performance of TPU on the fabrics as compared to the PLA [40]. Some studies have reported 3D printing of TPU on two different woven cotton

fabrics (thick and thin) and post-processing was performed using a heat press. After this, the adhesion test was performed in washing cycles. The results showed a higher adhesion on the thinner fabric and an increase in adhesion after one washing cycle [41]. Mukai et al. (2021) have prepared a wearable antenna for breast hypothermia applications by using 3D-printed TPU as a substrate [42]. In a similar study, an inkjet printer was used to print the silver ink on a polyester/cotton T-shirt, which enables tracking of the person who is wearing that T-shirt through a smartphone [43]. In another study, silver ink was printed on standard 65/35 polyester cotton fabric using an inkjet printer, which may be used as garments for medical and scientific applications [44].

The literature review reveals that numerous applications of MPA with a thermoplastic substrate (in wearable sensors) have been reported primarily due to its lightweight, flexibility, strength, and compactness. But up till now, little has been conveyed on the use of 3D printed TPU on CLW fabric-based substrate as a wearable sensor [38-44]. This study presents a novel and scalable approach for characterizing, simulating, and fabricating the substrate for wearable sensor applications. In this study 3D printing of TPU on CLW fabric (70% cotton (on the warp side) and -30% lycra (on the weft side) using the FFF process) has been reported (with a tradeoff between flexibility and strength), as a substrate for wearable sensor applications. The substrate has been explored for its rheological, mechanical, thermal, dielectric, RF, and 4D characteristics.

Materials and methods: Recycled (1°) TPU granules of 85 A shore hardness with MFI 29.758 g/(10 min) as per ASTM D 1238 (Table 1) have been selected.

Table 1: MFI observations for TPU granules

Trial No.	MFI in g/(10min)
1	29.916
2	28.6015
3	30.75
Average	29.758

The adopted methodology in this study is shown in Fig. 1. The reported literature highlight that different types of fabrics (Fig. 2) have been used for the direct printing of polymer as a substrate for wearable applications [35-37]. It has been reported that woven cotton fabric has shown better adhesion when a polymer is printed [36-38], therefore 70% cotton (for better crosslinking with polymer)-30% lycra (for stretchability) based woven fabric has been selected for this study (based on pilot experimentation). The TPU filament (ϕ1.75±0.05 mm) was fabricated on a single screw extruder (SSE) at 170°C temperature and 7 rpm (Fig. 3). Based on trial runs the parameters, and their levels were selected for 3D printing of TPU on FFF (Table 2). Table 3 shows a design of experiment (DOE) as per Taguchi L_9 orthogonal array (OA). Tensile samples (Fig. 4) according to ASTM D638 type-V were printed as per Table 3, which were further tested on a universal testing machine (UTM). The mechanical properties such as PS, stiffness, SE, and E has been tested (Fig. 5). Fig. 6 shows the true stress-true strain curve (as per Table 3).

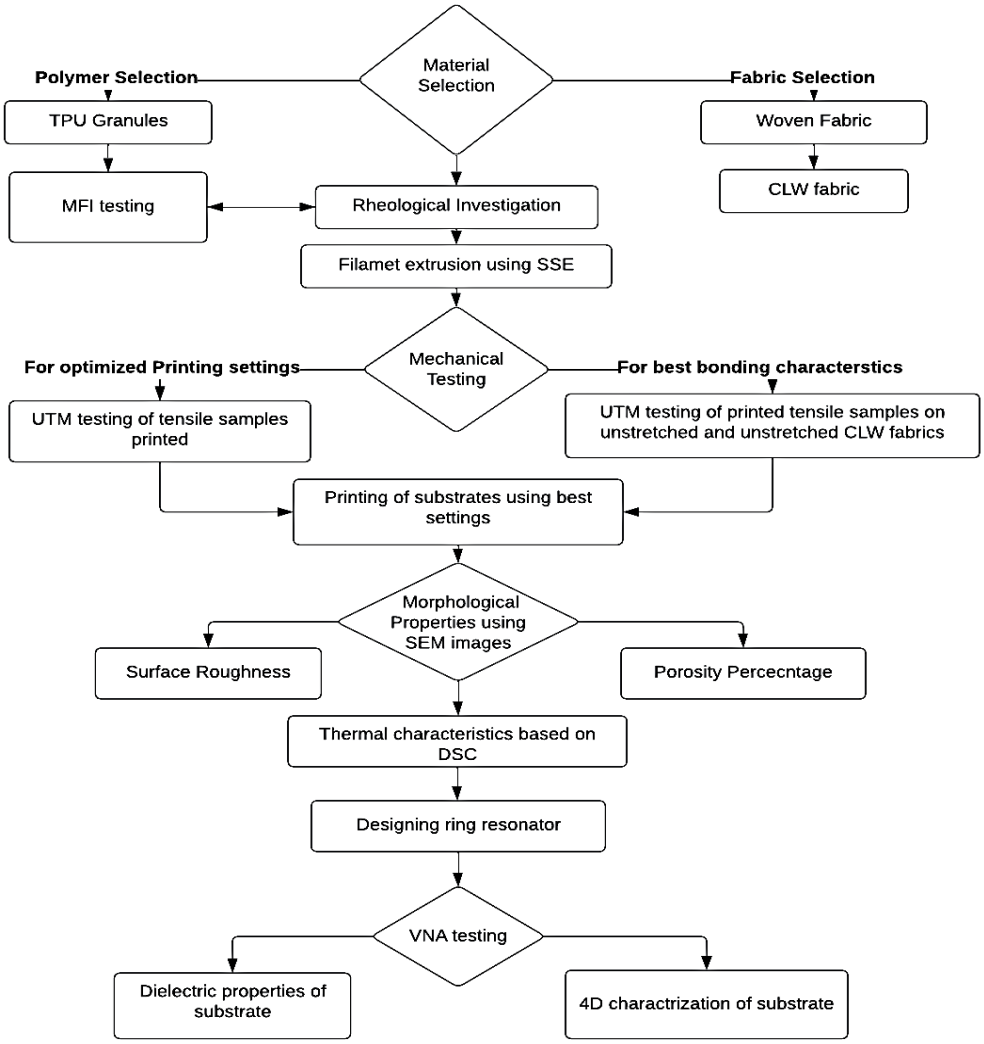

Fig. 1: Adopted methodology

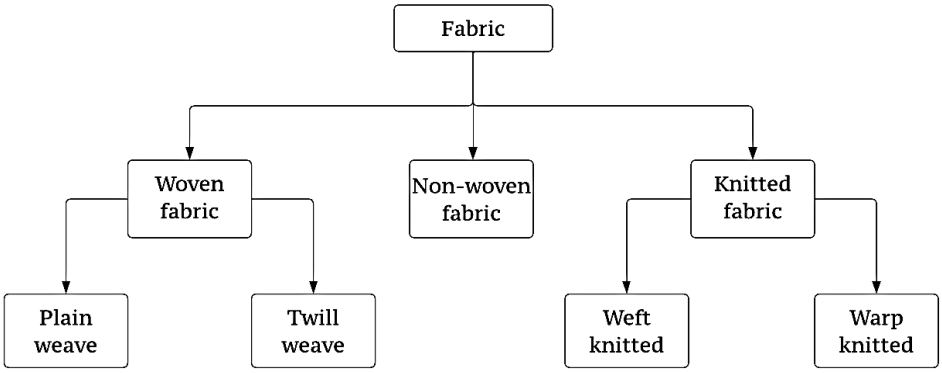

Fig. 2: Classification of fabric on basis of structure

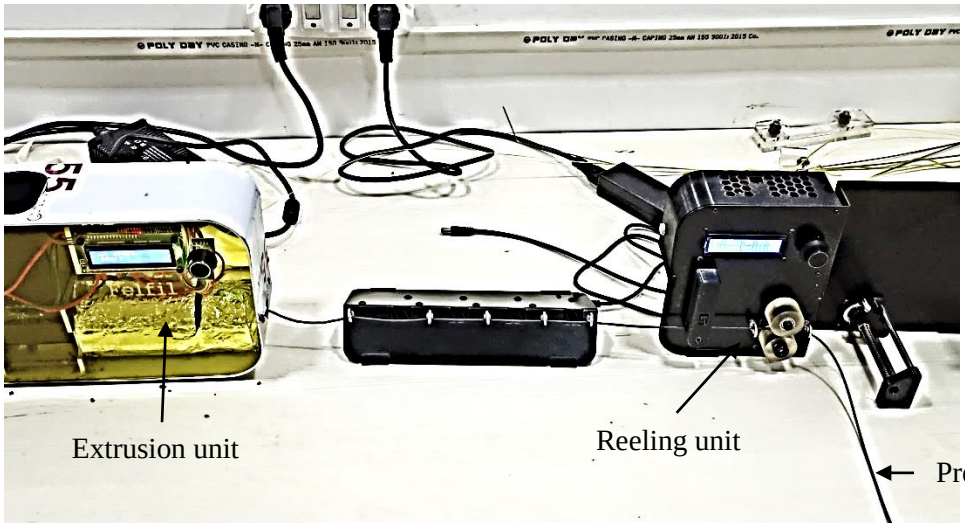

Fig. 3: Extrusion of TPU filament on SSE

Table 2: Selected parameters of FFF

Level	Inputs for FFF		
	A Nozzle temperature (°C)	B Printing speed (mm/s)	C Infill density (%)
1	215	15	100
2	220	18	80
3	225	21	60

Table 3: DOE followed for FFF

S. No.	Input parameters			Output parameters			
	A	B	C	PS (MPa)	Stiffness (N/mm)	SE (N.mm)	E (MPa)
S1	215	15	100	8.89±0.4	4.62±0.9	561.13±5.2	17±0.5
S2	215	18	80	8.73±0.9	4.09±1.0	546.46±6.1	15±1.0
S3	215	21	60	8.05±0.6	3.82±0.8	500.17±4.3	14±0.5
S4	220	15	80	8.27±0.6	3.89±0.7	531.24±3.8	15±0.5
S5	220	18	60	9.54±0.6	4.51±1.0	595.32±4.3	17±0.4
S6	220	21	100	7.46±0.7	4.12±0.8	478.89±5.6	15±0.5
S7	225	15	60	8.79±0.8	3.94±0.8	551.99±5.8	15±0.8
S8	225	18	100	8.89±0.8	4.05±0.9	555.76±6.2	15±0.4
S9	225	21	80	8.66±0.7	3.50±0.7	515.13±6.1	13±0.5

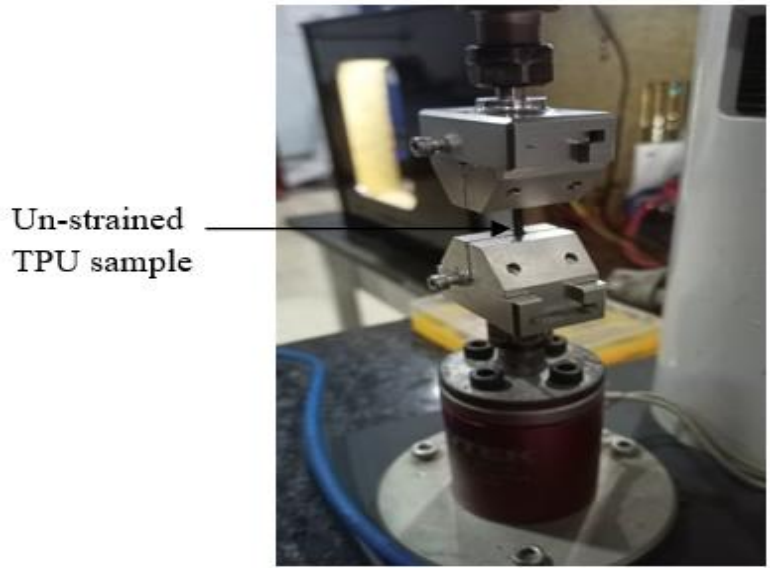

Fig. 4: Tensile testing strained conditions

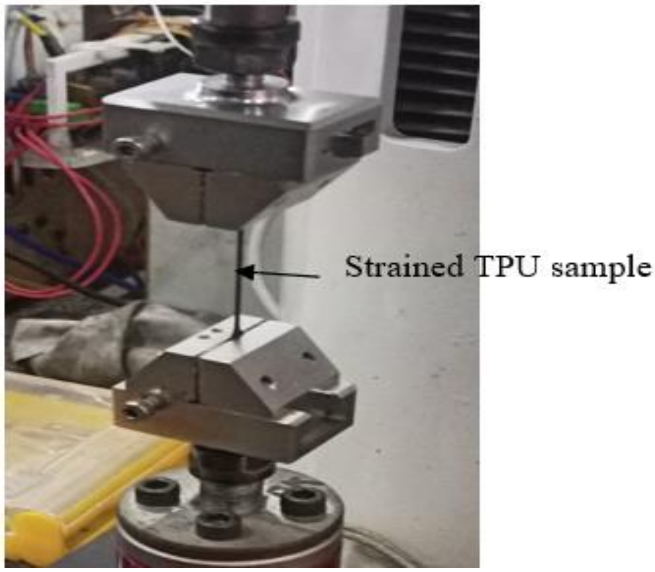

Fig. 5: Tensile testing strained conditions

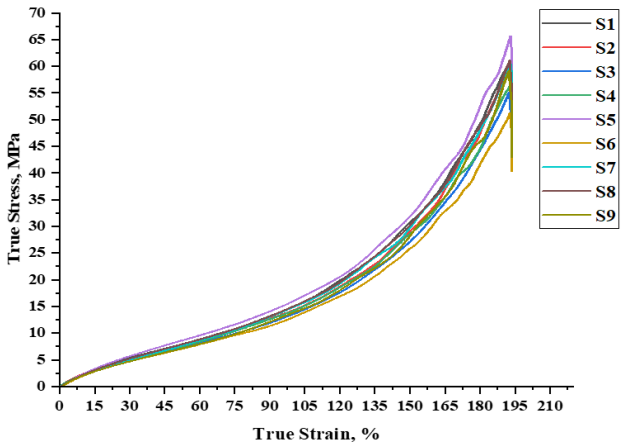

Fig. 6: True Stress True strain curve as per Table 4

Further for multifactor optimization, stiffness, SE, E, and PS (observed in Table 3) were analyzed by assigning the importance and weightage as shown in Table 5 and composite desirability was deduced.

Table 5: Output optimization: Stiffness, SE, E, and PS (based upon Table 4)

Output	Goal		Wt.%	Importance
Stiffness	Minimum		0.4	1
SE	Maximum		0.1	4
YM	Maximum		0.2	3
PS	Maximum		0.3	2
Solution			Composite Desirability	
A	B	C	0.931657	
3	2	3		

Based on Table 5, Fig 7 shows the optimization plot outlined that a printing temperature of 225˚C, printing speed of 18 mm/s, and infill density of 60% are the best settings. The sample was prepared at these proposed settings (from an optimization viewpoint) and corresponding 9.268 MPa PS, 3.311 N/mm stiffness, 525.687 N.mm SE, and 12 MPa E were observed.

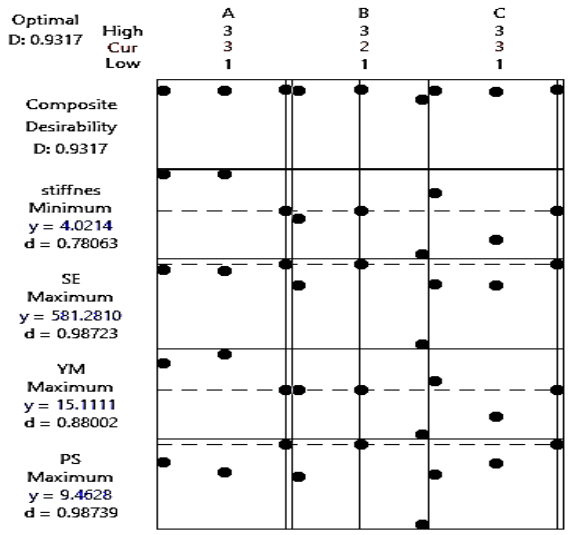

Fig. 7: Optimization plot for Stiffness, SE, E, and PS

The TPU tensile samples (with optimized settings: printing temperature of 225˚C, a printing speed of 18 mm/s, and infill density of 60%) were printed on stretched (from the weft side) and unstretched CLW fabric (Fig. 8), and mechanical properties were tested on UTM (Table 6). It was also observed that optimized printing settings of TPU on unstretched CLW fabric have shown less stiffness and high strain energy stored as compared to the TPU on stretched fabric, so the substrate of TPU was printed at optimized settings on unstretched fabric to provide more flexibility. Based on Table 6, the TPU substrate of size 60×54×0.65 mm (as per simulation of the RR in reported literature by using Ansys HFSS software [39]) was printed on unstretched CLW fabric at optimized settings (Fig. 9).

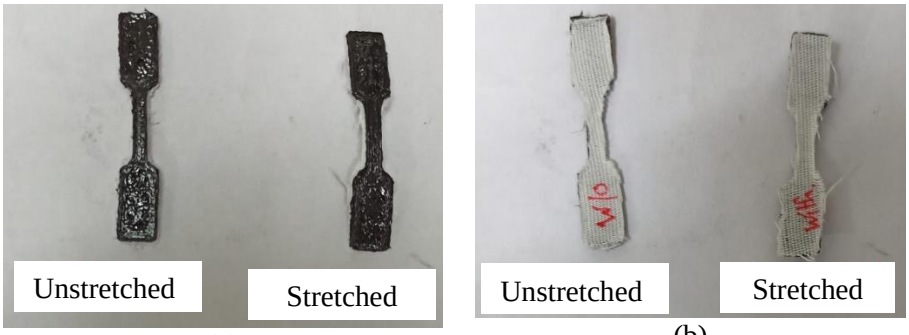

(a) (b)

Fig. 8: 3D printed tensile samples on unstretched and stretched CLW fabric front view (a) and back side view (b)

Table 6: Observed mechanical properties for TPU on stretched and unstretched CLW fabric

TPU printing on CLW fabric under	PS (MPa)	Stiffness (N/mm)	SE (N.mm)	E (MPa)
Stretched condition	6.6	6.658	107.378	21
Unstretched condition	5.675	3.829	500.177	14

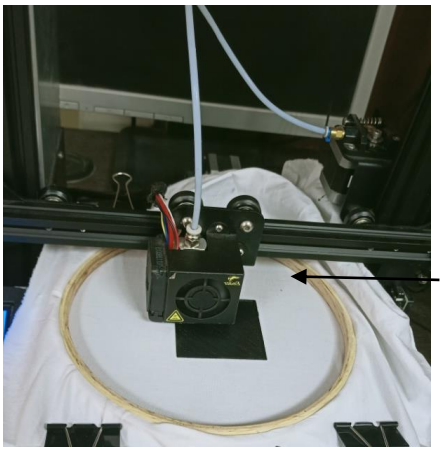

Fig. 9: 3D printing of TPU substrate on CLW fabric

Results and Discussion: The porosity analysis (as per ASTM B 276) was performed on SEM images. Fig. 10 and 11 respectively show SEM image and porosity% for samples S5, and S6 (with highest and lowest PS, SE respectively as per Table 3), and samples at optimized settings (at the cross-section and along the length). Based upon Fig. 10-11 it has been ascertained that observed mechanical properties (PS, SE) are in line with the observed porosity %.

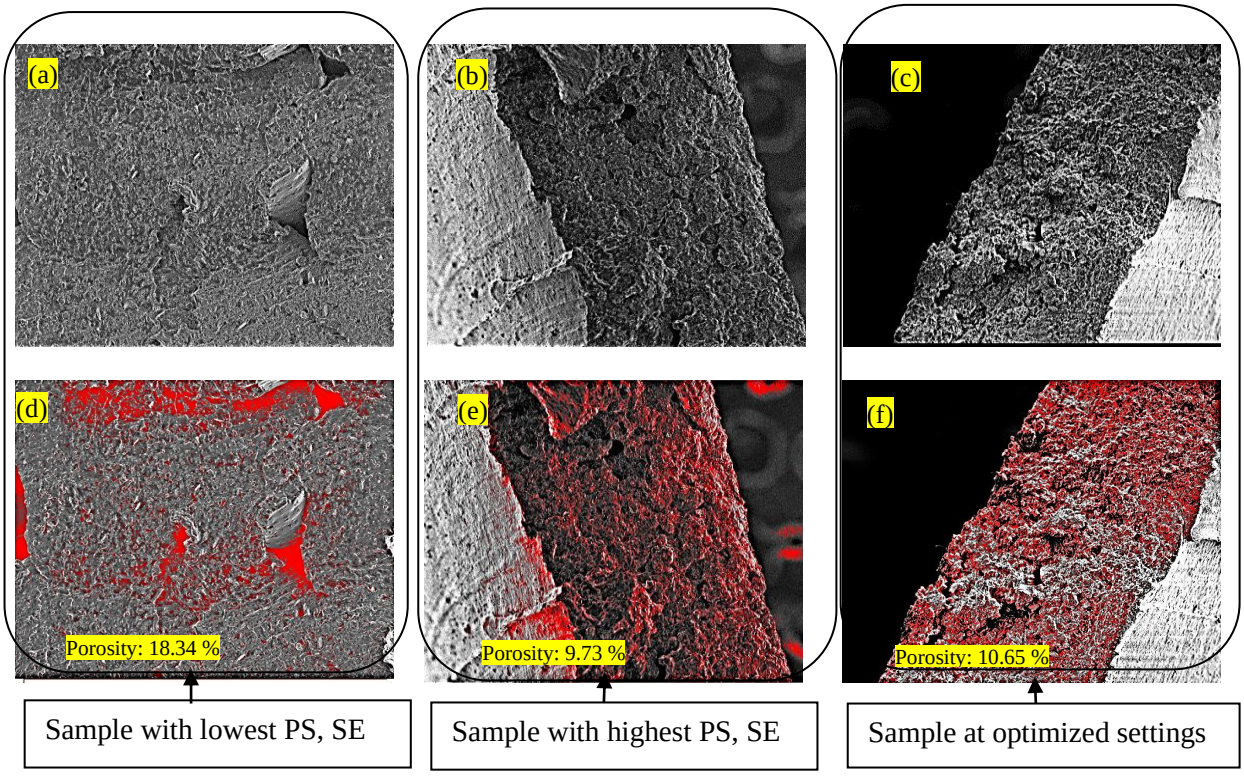

Fig. 10: SEM images (× 100) at the cross-section of sample S6 (a), sample S5 (b), and sample prepared at optimized settings (c), porosity% of sample S6 (d), porosity% of sample S5 (e) and porosity% of a sample prepared at optimized settings (f)

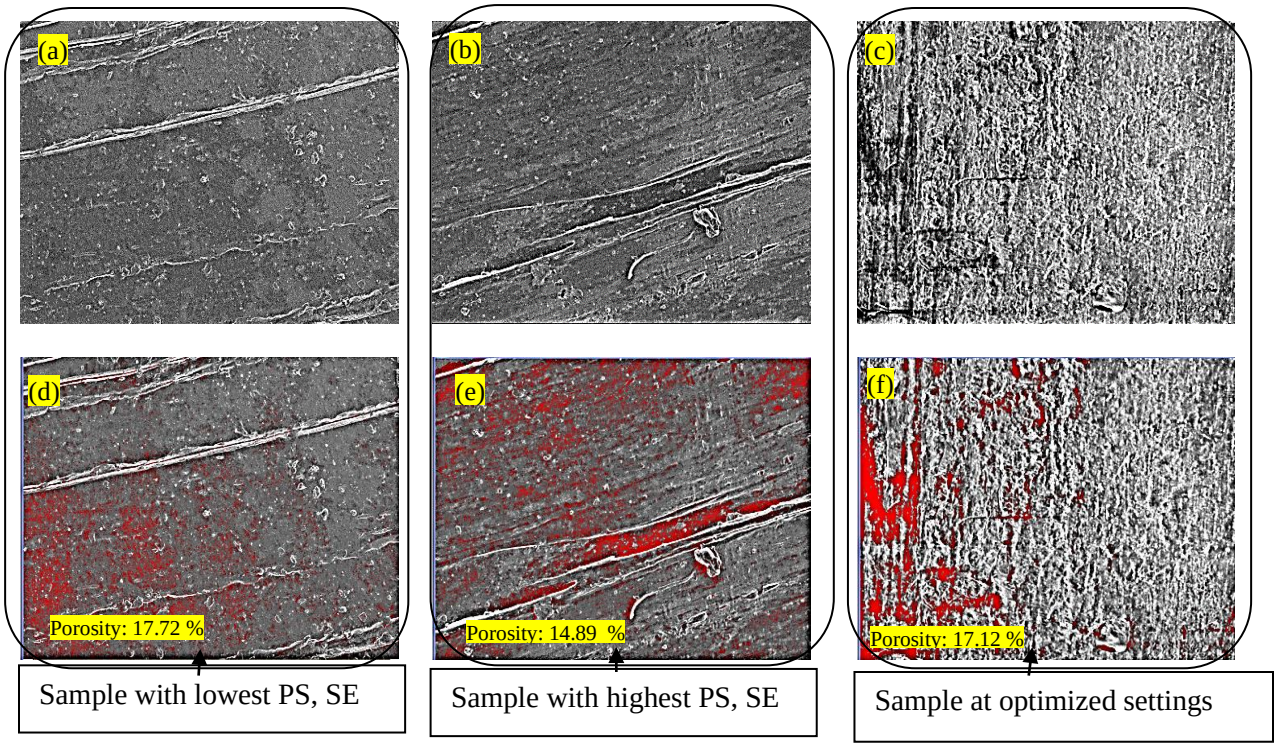

Fig. 11: SEM images (× 100) along the length of sample S6 (a), sample S5 (b), and sample prepared at optimized settings (c), porosity% of sample S6 (d), porosity% of sample S5 (e) and porosity% of a sample prepared at optimized settings (f)

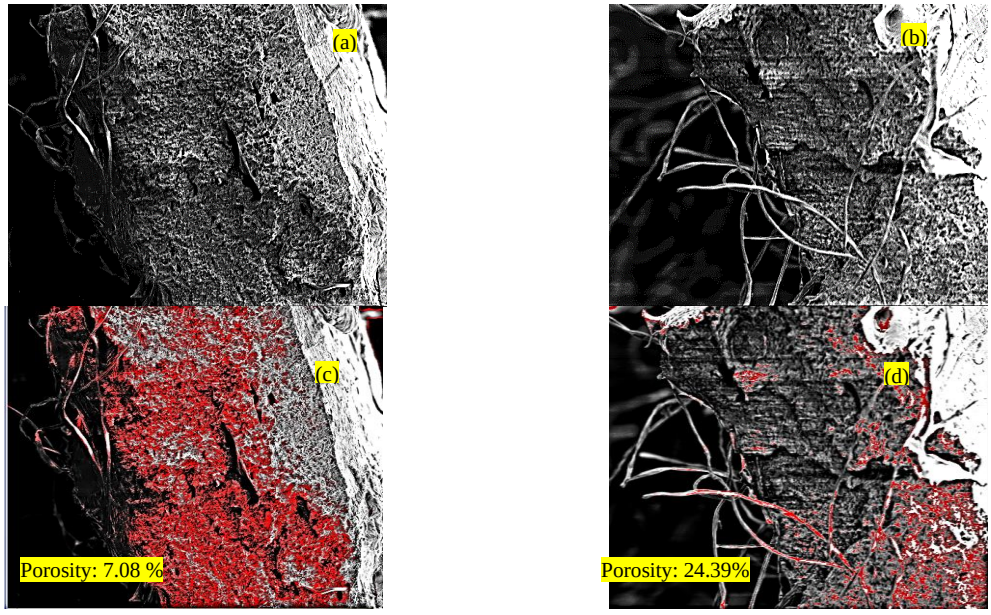

Fig. 12: SEM (×100) at a cross-section of samples printed on unstretched CLW fabric (a), stretched CLW fabric (b), porosity% of samples printed on unstretched CLW fabric (c), porosity% of samples printed on stretched CLW fabric (d)

Further, the SEM images of a tensile sample printed at optimized settings (on stretched and unstretched CLW fabric) at cross section and longitudinal section were processed for porosity analyses (Fig.12 and 13). Based on Fig. 12 and 13 it has been ascertained that TPU printing on CLW fabric in the unstretched condition is a better option from a morphological viewpoint.

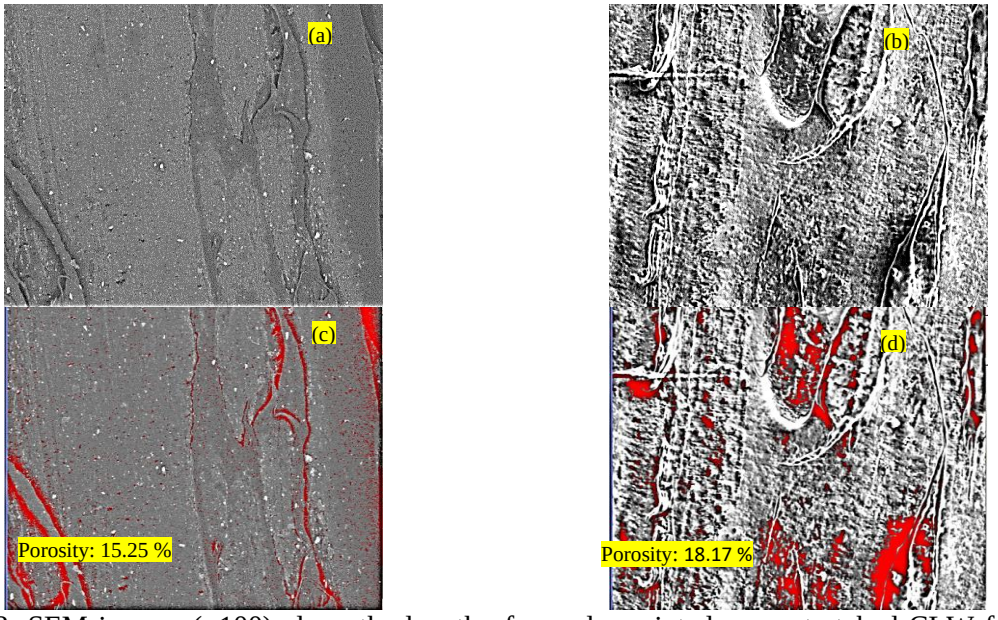

Fig. 13: SEM images (×100) along the length of samples printed on unstretched CLW fabric (a), stretched CLW fabric (b), porosity% of samples printed on unstretched CLW fabric (c), porosity% of samples printed on stretched CLW fabric (d)

For thermal characterization differential scanning calorimetry (DSC) was employed. Samples of TPU and TPU printed on CLW fabric were tested in a temperature range of 40-200°C with a rate of 10 K/min for 02 heating-cooling cycles as shown in Fig. 14. The first heating cycle showed that the glass transition (at first endothermic peak) of the TPU started at 40.01 °C to 42.25 °C whereas for TPU printed on CLW fabric the glass transition was observed from 49.01°C to 50.39 °C which shows a shift in the glass transition temperature denoting that the TPU printed on CLW fabric can be used at a little higher temperature. The second endothermic peak during the first heating cycle shows the melting of the polymer which was observed at 162°C with a heat consumption of 18.92 mJ for TPU and 161.11°C with a heat consumption of 4.60 mJ for TPU printed on CLW fabric. In the second heating cycle, there was an endothermic peak showing the melting of TPU at 161.07°C whereas TPU printed on CLW fabric has a peak at 160.45°C which represents heating and cooling have not affected the melting temperature of the TPU as well as TPU printed on CLW fabric. For wearable sensor applications, the DSC analyses were performed from 30-70°C for 3 heating and 3 cooling cycles as shown in Fig. 15. The endothermic peaks in the first heating cycle show the glass transition temperature. It was observed that the peaks have shown the same behavior during heating and cooling cycles which represents the thermal stability of both samples within this temperature range, hence may be used for wearable sensors in the selected temperature range.

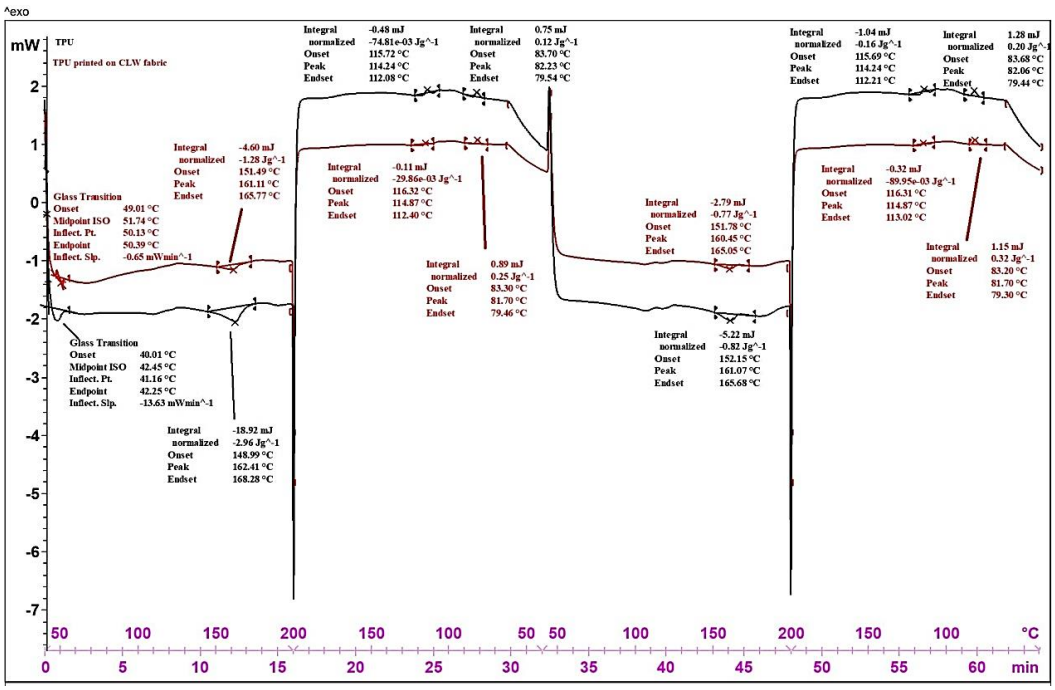

Fig. 14: DSC results for TPU and TPU printed on CLW fabric (Temperature ranging from 40°C to 200°C)

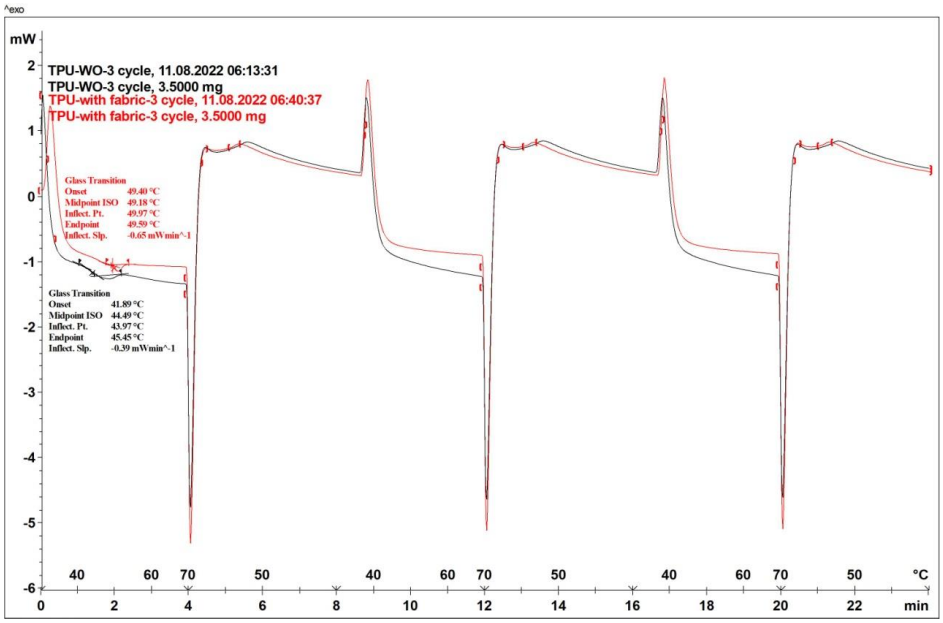

Fig. 15: DSC analyses of TPU and TPU printed on CLW fabric for wearable sensor applications (30°C to 70°C)

For the RF characterization and dielectric properties of the substrate, a RR was used to measure the ε_r and loss tangent ($\tan\delta$) of the substrate and 4D characteristics if any.

Initially ε_r as 2.5 was assumed (of the substrate) and the RR was designed for 2.45 GHz as per literature [45]. Table 7 shows the dimensions of the RR, further simulation of the RR was performed to check the dimensions (Fig. 16).

Table 7: Dimensions of RR with TPU printed on CLW fabric

Radius (mean)	13.50
Feed line width	1.91
Feed line length	10.82
Coupling gap	0.90
Substrate length	60.0
Substrate width	54.0
Inner ring radius	12.55
Outer ring radius	14.55

Note: All dimensions in mm

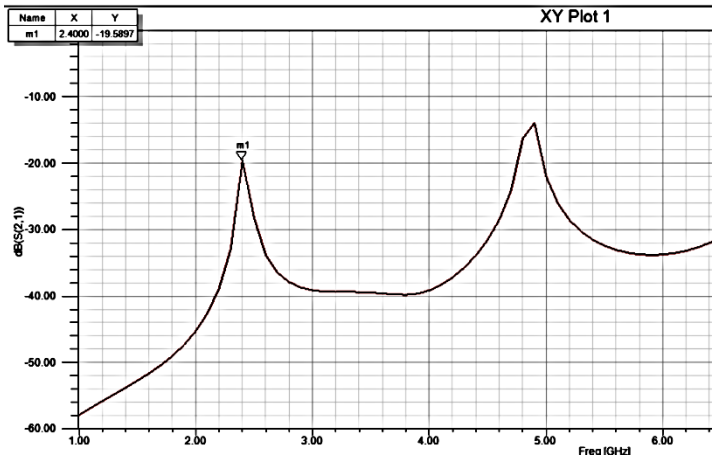

Fig. 16: Simulation of designed RR on HFSS

For a ring, feed lines, and ground plane, Cu tape (thickness 0.08 mm) was used. The right angles connectors (having an impedance load of 50Ω) (Fig. 17) were used in this study. The feed lines were pasted along the cotton (warp side) fibers to provide the strain in lycra fibers (weft side) for 4D characterization without disturbing the coupling gap between the feed lines and ring.

(a) Pasting Ring and feed lines

(b) Pasting copper tape as ground

(c) Soldering connector with ground

(d) Soldering Connector with Feed lines

Fig. 17: RR patch on the substrate

For further analysis, the transmission coefficient (S_{21}) was measured using VNA. It was observed that the RR, when unloaded was resonating at 2.85 GHz with an insertion loss of -35.72 dB, and the RR based on a substrate when loaded till 24.36 N gives a displacement of 1 mm in the substrate and then it resonated at 2.6531 GHz with an insertion loss of -70.11dB. The same cycle has been repeated again and under unloaded conditions, RR resonated at 2.85 GHz and when loaded to 24.36 N it resonated at 2.6554 GHz. The controlled RF shift (Fig. 18) ascertains the 4D characteristics of the substrate.

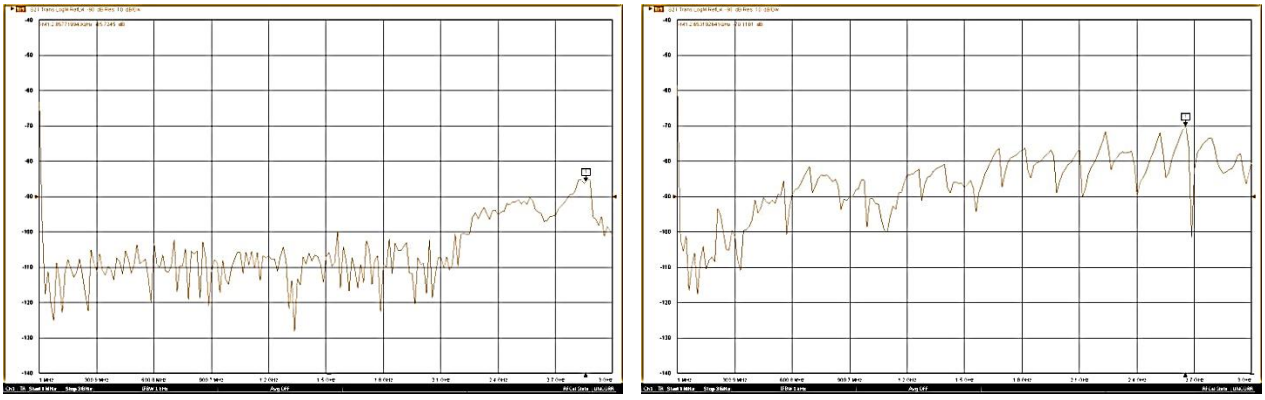

(a) (b)

Fig. 18: Observed S_{21} of TPU-CLW fabric-based RR unloaded(a) and with a load of 24.36 N (b)

The ε_r and $\tan\delta$ for substrate (TPU on CLW fiber) were calculated (Table 8) based on the reported literature [45, 46].

Table 8: Calculated RF, ε_r and tan δ under cyclic loading

Cycles	Loading condition	RF (GHz)	ε_r	tan δ
Cycle 1	Unloaded	2.85	1.74	0.0047
	Load of 25N	2.6531	2.07	0.0049
Cycle 2	Unloaded	2.85	1.74	0.0047
	Load of 25N	2.6554	2.06	0.0049

The controlled variation in ε_r of the substrate upon cyclic loading highlights its 4D property, as this results in programable RF output in the ISM band. It may be noted that for ensuring the reliability of the functional prototype, the samples were loaded and unloaded for two consecutive cycles (with 03 repetitions). It was observed that the Cu tape used as a conductor started separation from the substrate after three cycles. For field applications requiring repeatability and reliability, the higher number of cycles (say 50-100) needs to be explored. In that situation, for further cyclic loading silver ink may be printed on the TPU instead of Cu tape.

To ascertain the effect of the human body on the sensor performance, the RR was mounted on the biceps and stomach and the RF characteristics were measured using VNA (Fig.19). It was observed that there has been a change in the RF from 2.85 GHz to 2.72 GHz when applied on the body.

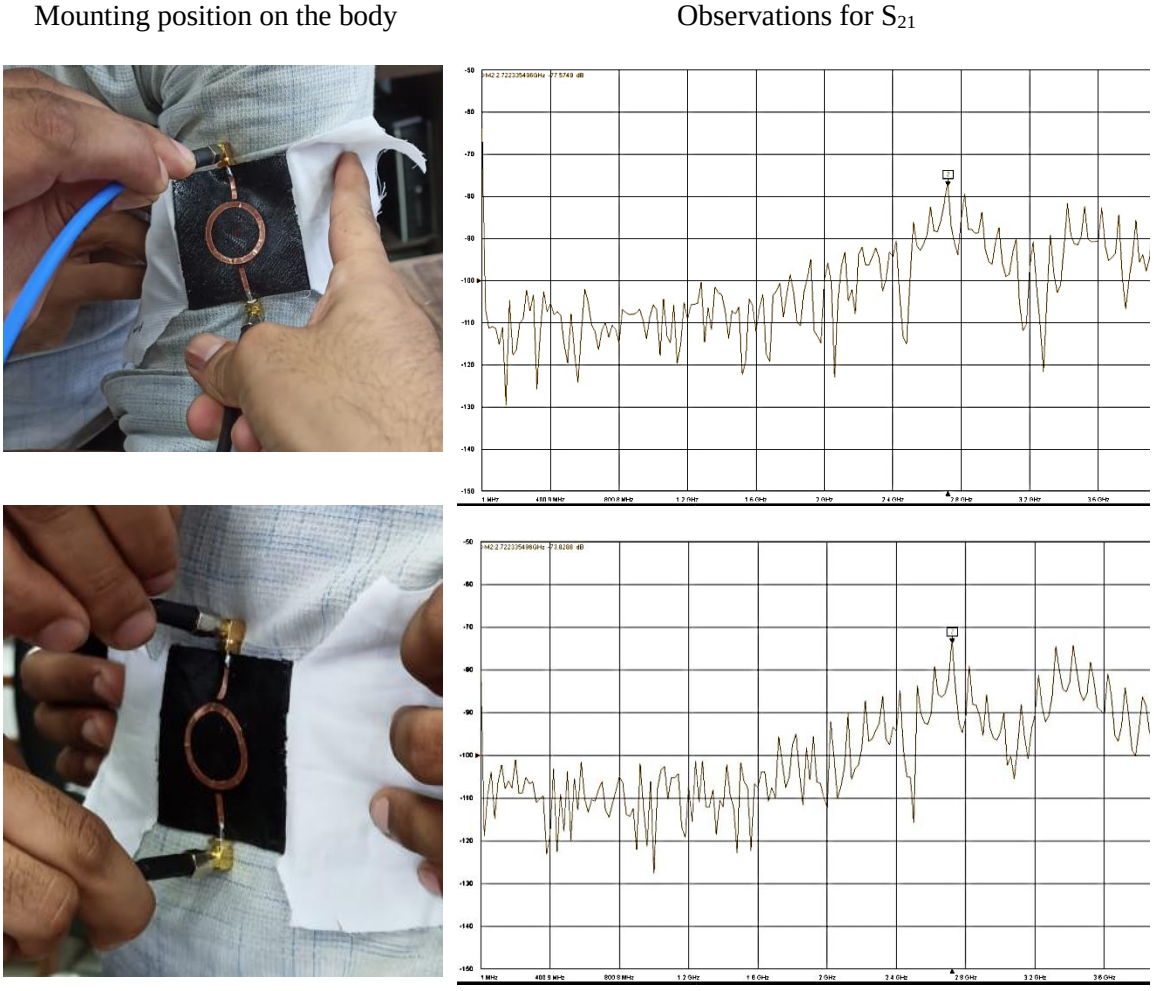

Fig. 19: Observed S_{21} values while mounting on body parts: biceps (a) and stomach (b)

Table 9 shows the properties of different tissues (to resemble the human body) which were used to measure the specific absorption rate (SAR) value simulated by using HFSS (Fig. 20) as 0.004 W/kg over 1g tissue which is well under permissible limits. So, the purposed functional prototype may be used in wearable applications.

Table 9: Properties of different body tissues for SAR value calculation [47, 48]

Body tissue layer	Permittivity	Conductivity (S/m)	Density (kg/m^3)	Body tissue layer thickness for simulation (mm)
Skin	38.007	1.464	1020	1.7
Fat	5.280	0.105	918	8
Muscle	53.574	1.810	1040	10

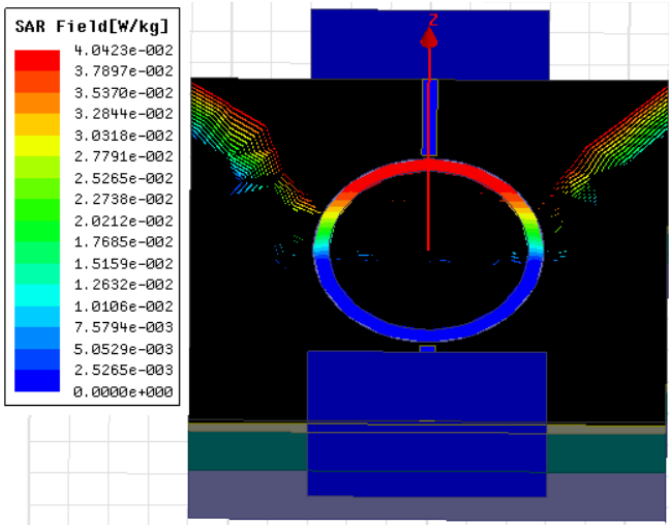

Fig. 20: SAR value of RR

It was also observed that the TPU-CLW fabric-based substrate has shown more ε_r as compared to the other materials reported in previous literature [49] and has lower ε_r as compared to the commercially available thermoplastics available as shown in Table 10. Yet the lower ε_r leads to higher bandwidth and higher gain but the higher ε_r leads to less size of the patch antenna which makes it easy to be used in wearable sensor applications as they provide fewer disturbances to the wearer. Hence, the proposed substrate has provided higher gain and bandwidth with a decrease in size.

Table 10: Relative permittivity of different fabrics measured at 2.45GHz

Materials	Substrate material	ε_r
Fabrics	Polyester	1.44
	Bed sheet	1.46
	Curtain Cotton	1.47
	Wash jeans	1.51
	Polycot	1.56

	Jeans Cotton	1.67
TPU+CWL fabric	Proposed Substrate	1.74
Thermoplastics [50-51]	FR4	4.36
	Teconic TLC	3.2
	RT Duroid	2.2
	ABS	2.74

From a practical application viewpoint the passive sensor in this study requires the following properties:

- Repeatability (4D characteristics, tested for loading and unloading cycles, and the repeatability was observed)
- Reliability (assured by repeated loading and unloading of the sensor)
- Sensing capabilities (checked by using VNA)
- Minimal need for special hardware/ software (a sensor may be directly wearable and observations may be noted by smartphone)

It may be noted that 3D printing is not for mass production. In this study, customized prototypes for the wearable sensors were prepared, which may be further manufactured with different techniques for mass production. The passive sensor may be easily integrated into the clothes and may be applied on the body (on the wrist, thigh, knee, leg, etc.) as per required applications.

Conclusions: -

→ Recycled TPU was successfully printed on the CLW fabric by FFF, which may be used as a wearable sensor. TPU is one of the flexible 3D printable materials with shape memory properties, hence may be used for 4D characterizations.

→ In this study, the optimized settings for printing recycled TPU were ascertained based on mechanical testing as 225°C nozzle temperature, 18 mm/s printing speed, and 60% infill density.

→ Dielectric properties (ε_r) of TPU printed on CLW fabric (combined) were calculated which comes out to be 1.74, hence may be used to provide a balance among the size, gain, and bandwidth of the sensor.

→ The substrate has shown the 4D characteristics with a change in RF when a load was applied from 0-25 N, resulting in programable RF output in the ISM band.

→ The proposed 3D printed sensors may be used to sense movements (in arms, legs, muscles, etc.), abnormal swelling/ condition/ health monitoring (of sportspersons) while training, tracking of humans/animals, etc. by configuring the same in ISM band.

References

1. Tsolis A, Whittow WG, Alexandridis AA, et al. Embroidery and related manufacturing techniques for wearable antennas: Challenges and opportunities. Electronics 2014; 3:314–338 DOI: 10.3390/electronics3020314.
2. Ramadan M and Dahle R Characterization of 3-D Printed Flexible Heterogeneous Substrate Designs for Wearable Antennas. IEEE Trans. Antennas Propag. 2019; 67: 2896–2903 DOI: 10.1109/TAP.2019.2896762.
3. Simorangkir RBVB, Yang Y, Esselle KP, et al. A Method to Realize Robust Flexible Electronically Tunable Antennas Using Polymer-Embedded Conductive Fabric. IEEE Trans. Antennas Propag. 2018; 66: 50–58 DOI: 10.1109/TAP.2017.2772036.

4. Mohamadzade B, Hashmi RM, Simorangkir RBVB, et al. Recent advances in fabrication methods for flexible antennas in wearable devices: State of the art. Sensors (Switzerland) 2019; 19: 10 DOI: 10.3390/s19102312.
5. Roy S and Chakraborty U Metamaterial Based Dual Wideband Wearable Antenna for Wireless Applications. Wirel. Pers. Commun.2019; 106:1117–1133 DOI: 10.1007/s11277-019-06206-3.
6. Abbas SM, Esselle KP, and Ranga Y An armband-wearable printed antenna with a full ground plane for body area networks. IEEE Antennas Propag. Soc. AP-S Int. Symp. 2014; DOI: 10.1109/APS.2014.6904491.
7. Njogu P, Sanz-Izquierdo B, Elibiary A, et al. 3D Printed Fingernail Antennas for 5G Applications. IEEE Access 2020; 8: 228711–228719 DOI: 10.1109/ACCESS.2020.3043045.
8. Njogu P, Sanz-Izquierdo B, Elibiary A, et al. Stability and efficiency of screen-printed wearable and washable antennas. IEEE Antennas Wirel. Propag. Lett. 2012; 11:838–841 DOI: 10.1109/LAWP.2012.2207941.
9. Lim C, Shin Y, Jung J, et al. Stretchable conductive nanocomposite based on alginate hydrogel and silver nanowires for wearable electronics. APL Materials 2019; DOI: 10.1063/1.5063657.
10. Raval S and Raval F Wearable -Textile Patch Antenna using Jeans as Substrate at 2.45 GHz. IJERT 2014; DOI: 10.17577/IJERTV3IS050548.
11. Khan MUA, Raad R, Tubbal F, et al. Bending Analysis of Polymer-Based Flexible Antennas for Wearable, General IoT Applications : A Review. Polymers (Basel) 2021; 13: 357.
12. Salonen P, Kim J, and Rahmat-Samii Y Dual-band E-shaped patch wearable textile antenna. IEEE Antennas Propag. Soc. AP-S Int. Symp. 2005; 1:466–469 DOI: 10.1109/APS.2005.1551354.
13. Anagnostou DE, Gheethanet AA, Amert AK, et al. A direct-write printed antenna on paper-based organic substrate for flexible displays and WLAN applications. IEEE/OSA J. Disp. Technol. 2010; 6:558–564 DOI: 10.1109/JDT.2010.2045474.
14. Sallam MO, Kandil SM, Volski V, et al. Wideband CPW-Fed Flexible Bow-Tie Slot Antenna for WLAN/WiMax System. IEEE Transactions On Antennas And Propagation 2017; 65:4274–4277.
15. Pei R, Leach M, Lim EG, et al. Wearable EBG-Backed Belt Antenna for Smart On-Body Applications. IEEE Trans. Ind. Informatics 2020; 16:7177–7189 DOI: 10.1109/TII.2020.2983064.
16. Singh T, Kumar S and Sehgal S 3D printing of engineering materials: A state of the art review. Mater. Today Proc. 2020; 28:1927–1931 DOI: 10.1016/j.matpr.2020.05.334.
17. Ahmed W, Ahmed S and Alnajjar F Mechanical performance of three-dimensional printed sandwich composite with a high-flexible core. Proc. Inst. Mech. Eng. Part L J. Mater. Des. Appl.2021;235:1382–1400 DOI: 10.1177/14644207211011729.
18. Rodrigues D, Belinha1 J and Jorge1 RMN The elastoplastic analysis of 3D-printed thermoplastics using the NNRPIM and a modified hill yield criterion. Proc. Inst. Mech. Eng. Part L J. Mater. Des. Appl.2021;235:1368–1381 DOI: 10.1177/1464420720985890.
19. Pais A , Silva C, Marques MC, et al. The influence of infill density gradient on the mechanical properties of PLA optimized structures by additive manufacturing. Proc. Inst. Mech. Eng. Part L J. Mater. Des. Appl. 2021; 235:1401–1418 DOI: 10.1177/14644207211007159.
20. Mirzaee M and Noghanian S Additive manufacturing of a compact 3D dipole antenna using ABS thermoplastic and high-temperature carbon paste. IEEE Antennas Propag. Soc. Int. Symp. APSURSI 2016 - Proc. 2016;1:475–476 DOI: 10.1109/APS.2016.7695946.
21. Whittow WG 3D printing, inkjet printing, and embroidery techniques for wearable antennas.10th Eur. Conf. Antennas Propagation EuCAP 2016; DOI: 10.1109/EuCAP.2016.7481266.
22. Tan HW, An J, Chua CK, et al. Metallic Nanoparticle Inks for 3D Printing of Electronics. Adv. Electron. Mater.2019; 5:5. DOI: 10.1002/aelm.201800831.
23. Hoyack M, Bjorgaard J, Huber E, et al. Connector design for 3D printed antennas. IEEE Antennas Propag. Soc. Int. Symp. APSURSI 2016 - Proc. 2016; pp. 477–478 DOI: 10.1109/APS.2016.7695947.

24. McKerricher G, Titterington D and Shamim A A Fully Inkjet-Printed 3-D Honeycomb-Inspired Patch Antenna. IEEE Antennas Wirel. Propag. Lett. 2016; 15:544–547, DOI: 10.1109/LAWP
25. Jun S, Elibiary A, Sanz-Izquierdo B, et al. 3-D printing of conformal antennas for diversity wrist worn applications. IEEE Trans. Components, Packag. Manuf. Technol.2018; 8:2227–2235 DOI: 10.1109/TCPMT.2018.2874424.
26. Farooqui MF and Shamim A Dual-band inkjet printed bow-tie slot antenna on leather. 7th Eur. Conf. Antennas Propagation, EuCAP 2013; pp. 3287–3290.
27. Rizwan M, Khan WA, Sydanheimo L, et al. Flexible and Stretchable Brush-Painted Wearable Antenna on a Three-Dimensional (3-D) Printed Substrate. IEEE Antennas Wirel. Propag. Lett. 2017; 16:3108–3112 DOI: 10.1109/LAWP.2017.2763743.
28. Moscato S, Bahr R, Le T, et al. Infill-Dependent 3-D-Printed Material Based on NinjaFlex Filament for Antenna Applications. IEEE Antennas Wirel. Propag. Lett. 2016; 15:1506–1509 DOI: 10.1109/LAWP.2016.2516101.
29. Tian M, Yao Y, Liu S, et al. Separated-structured all-organic dielectric elastomer with large actuation strain under ultra-low voltage and high mechanical strength. J. Mater. Chem. A Mater. energy Sustain 2014; DOI: 10.1039/C4TA04197F.
30. Tayfun U and Kanbur Y Mechanical, electrical and melt flow properties of polyurethane elastomer / surface-modified carbon nanotube composites. Journal of Composite Materials 2016; DOI: 10.1177/0021998316666158.
31. He X, Zhou J, Jin L, et al. Improved Dielectric Properties of Thermoplastic Polyurethane Elastomer Filled with Core – Shell. Materials (Basel) 2020; DOI: 10.3390/ma13153341.
32. Mukai Y, Li S and Suh M. 3D-printed thermoplastic polyurethane for wearable breast hyperthermia. Fash. Text. 2021; DOI: 10.1186/s40691-021-00248-7.
33. Varkiani SMH and Afsahi M Compact and ultra-wideband CPW-fed square slot antenna for wearable applications. AEU - Int. J. Electron. Commun. 2019; DOI: 10.1016/j.aeue.2019.04.024.
34. Wu L, Huang J, Zhai M, et al. Deformable bowtie antenna realized by 4d printing. Electronics 2021; DOI: 10.3390/electronics10151792.
35. Ahmed MI, Ahmed MF, and Shaalan AA Novel electrotextile patch antenna on jeans substrate for wearable applications. Prog. Electromagn. Res. C 2018; DOI: 10.2528/PIERC18030309.
36. Spahiu1T, Al-Arabiyat M, Martens Y, et al. Adhesion of 3D printing polymers on textile fabrics for garment production Adhesion of 3D printing polymers on textile fabrics for garment production. Aegean International Textile and Advanced Engineering Conference 2018; DOI: 10.1088/1757-899X/459/1/012065.
37. Pei E, Shen J and Watling J Direct 3D printing of polymers onto textiles : experimental studies and applications. Rapid Prototyping Journal 2015; DOI: 10.1108/RPJ-09-2014-0126.
38. Nacer C, Zhadobov M, Le Coq L, et al. Wearable endfire textile antenna for on-body communications at 60 GHz. IEEE Antennas Wirel. Propag. Lett. 2012; DOI: 10.1109/LAWP.2012.2207698.
39. Martens Y, Ehrmann A. Composites of 3D-printed polymers and textile fabrics. In IOP Conference Series: Materials Science and Engineering 2017 Aug 1 (Vol. 225, No. 1, p. 012292). IOP Publishing.
40. Oyon Calvo J, Cazon Martin A, Rodriguez Ferradas MI, et al. Additive manufacturing on textiles with low-cost extrusion devices: Adhesion and deformation properties. Dyna. 2019 Mar 1;94(2):221-5.
41. Störmer J, Görmer D, Ehrmann A. Influence of washing on the adhesion between 3D-printed TPU and woven fabrics. Communications in Development and Assembling of Textile Products. 2021 Jun 9;2(1):34-9.
42. Mukai Y, Li S, Suh M. 3D-printed thermoplastic polyurethane for wearable breast hyperthermia. Fashion and Textiles. 2021 Dec;8(1):1-2.

43. Krykpayev B, Farooqui MF, Bilal RM, Vaseem M, Shamim A. A wearable tracking device inkjet-printed on textile. Microelectronics Journal. 2017 Jul 1;65:40-8.
44. Whittow WG, Chauraya A, Vardaxoglou JC, Li Y, Torah R, Yang K, Beeby S, Tudor J. Inkjet-printed microstrip patch antennas realized on textile for wearable applications. IEEE Antennas and Wireless Propagation Letters. 2014 Jan 2;13:71-4.
45. Singh R, Kumar S, Singh AP, et al. On comparison of recycled LDPE and LDPE–bakelite composite based 3D printed patch antenna. Proc. Inst. Mech. Eng. Part L J. Mater. Des. Appl. 2022; DOI: 10.1177/14644207211060465.
46. Yang L, Rida A, Vyas R, et al. RFID tag and RF structures on a paper substrate using inkjet-printing technology. IEEE Trans. Microw. Theory Tech. 2007; DOI: 10.1109/TMTT.2007.909886.
47. Singh G and Kaur J. Skin and brain implantable inset-fed antenna at ISM band for wireless biotelemetry applications. Microwave and Optical Technology Letters. 2021; 63(2):510-5.
48. Yalduz H, Tabaru TE, Kilic VT, et al. Design and analysis of low profile and low SAR full-textile UWB wearable antenna with metamaterial for WBAN applications. AEU-International Journal of Electronics and Communications. 2020; 126:153465.
49. Sankaralingam S and Gupta B Determination of dielectric constant of fabric materials and their use as substrates for design and development of antennas for wearable applications. IEEE Trans. Instrum. Meas. 2010; DOI: 10.1109/TIM.2010.2063090.
50. Khan A and Nema R Analysis of Five Different Dielectric Substrates on Microstrip Patch Antenna. International Journal of Computer Applications 2012; 55: 0975 – 8887.
51. Malek NA, Ramly AM, Sidek A, et al. Characterization of Acrylonitrile Butadiene Styrene for 3D Printed Patch Antenna. Indonesian Journal of Electrical Engineering and Computer Science 2017; 6:116-123.